Theory of resonance fluorescence from a solid-state cavity QED system: Effects of pure dephasing

Kazuki Koshino

College of Liberal Arts and Sciences, Tokyo Medical and Dental University, 2-8-30 Konodai, Ichikawa 272-0827, Japan

(Received 15 June 2011; published 15 September 2011)

We theoretically analyze the resonance fluorescence of a solid-state cavity quantum electrodynamics (QED) system that consists of a quantum dot and a cavity. We clarify the effects of pure dephasing by investigating the elastic and inelastic scattering probabilities, the fluorescence power spectrum, and the energy exchange with the environment. Pure dephasing interactions with the environment both enhance nonresonant coupling between the dot and the cavity and enable the pump light to continuously absorb energy from the environment under appropriate conditions.

DOI: 10.1103/PhysRevA.84.033824 PACS number(s): 42.50.Ct, 42.50.Pq

I. INTRODUCTION

Indistinguishable single photons that undergo perfect two-photon interference are the key physical resource for optical quantum information processing [1]. It is thus critical to develop techniques for high-fidelity deterministic generation of such single photons [2–5]. Cavity quantum electrodynamics (QED) systems are promising for deterministically generating single photons. In these systems, spontaneous emission from a single emitter is predominantly forwarded to a one-dimensional field (the radiation pattern of the cavity) due to the Purcell effect [6]. Cavity QED systems have been realized in various physical systems, including real atoms in Fabry-Perot or toroidal cavities [7–9], semiconductor quantum dots in planar or photonic crystal cavities [10,11], and superconducting qubits coupled to a microwave transmission line [12,13]. The principal advantage of systems employing real atoms or molecules is the long quantum coherence times of the atoms and the cavity photons. In contrast, solid-state cavity QED systems have practical advantages such as dominant coupling to a one-dimensional external field [14] and spatial compactness. These advantages make them suitable for constructing scalable quantum networks.

A recent hot topic in the field of solid-state cavity QED systems is nonresonant coupling between the quantum dot and the cavity. In several experiments, strong emission has been observed at the cavity frequency, although the pump laser is tuned to the dot that has a large detuning from the cavity [15–19]. This phenomenon has not been observed in atomic cavity QED systems and is considered to be unique to solid-state systems. Recent theoretical studies have investigated radiative decay of an excited dot coupled to a cavity and have clarified the effects of pure dephasing on the spontaneous-emission power spectrum [20–22]. The emitted photon spectrum obeys the following formula [20,23]:

$$S_{\rm se}(\omega) \propto |(\omega-\widetilde{\omega}_d)(\omega-\widetilde{\omega}_c)-g^2|^{-2}, \tag{1}$$

where $\widetilde{\omega}_d$ and $\widetilde{\omega}_c$ are the complex frequencies of the dot and cavity, respectively. When the dot linewidth is much narrower than the cavity linewidth ($\mathrm{Im}\,\widetilde{\omega}_d \ll \mathrm{Im}\,\widetilde{\omega}_c$), as is the case in atomic cavity QED systems, a dominant peak of $S_{\rm se}(\omega)$ appears at the dot frequency. In contrast, when the dot linewidth far exceeds the cavity linewidth due to pure dephasing ($\mathrm{Im}\,\widetilde{\omega}_d \gg \mathrm{Im}\,\widetilde{\omega}_c$), a dominant peak appears at the cavity frequency. This partly explains the experimentally observed strong emission at the cavity frequency in solid-state cavity QED systems.

In actual experiments, a continuous laser beam is commonly employed as a pump and resonance fluorescence from the system is measured in the stationary state. The spontaneous-emission and resonance fluorescence spectra are expected to be strongly related, but their quantitative relationship is still unclear. Resonance fluorescence consists of coherent and incoherent components (i.e., elastically and inelastically scattered light), but the spontaneous-emission spectrum apparently has no connection with the coherent component. Furthermore, regarding the incoherent component, strong-field effects such as Mollow triplets and stimulated emission can never appear in $S_{\rm se}(\omega)$. The objective of this study is to quantitatively analyze resonance fluorescence from solid-state cavity QED systems and to reveal the effects of strong pure dephasing of the dot induced by the solid-state environments. In this study, we treat the five elements of the overall system (dot, cavity, leakage from cavity, noncavity radiation of the dot, and pure dephasing of the dot due to the environment) as active quantum-mechanical degrees of freedom. By rigorously solving the resultant Heisenberg equations, we present numerical results for the elastic and inelastic scattering probabilities and the power spectrum of the cavity radiation. Furthermore, we show that the pump light can absorb energy from the environment through pure-dephasing coupling under appropriate conditions.

The effects of pure dephasing have been investigated intensively in atomic cavity QED systems in light of quantum nondemolition measurements [24–29]. The differences between these works and the present one are as follows: In Refs. [24–29], the atom is used as a probe for inferring the quantum state of cavity photons and interacts with intracavity photons without being pumped. The main concern of these studies is the correlation between the atomic and photonic states generated by their interaction. In contrast, in this study, the quantum dot is pumped continuously by an external laser. We are mainly concerned with the stationary optical response of the dot-cavity system and investigate the quantum-mechanical properties of resonance fluorescence from this system.

The remainder of this paper is organized as follows: We present the theoretical model in Sec. II and the resultant Heisenberg equations in Sec. III. We discuss the correlation

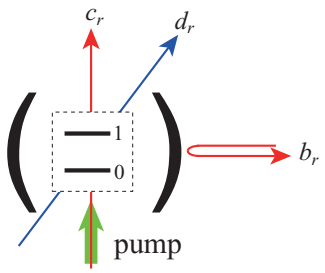

FIG. 1. (Color online) Schematic illustration of the solid-state cavity QED system considered. It consists of a quantum dot, a cavity, leakage from the cavity (b field), noncavity radiation modes (c field), and the environment that causes pure dephasing of the dot (d field). The pump light is input from the c field. The coupling constants are defined in the text.

functions of system operators in Sec. IV and present analytic and numerical results for the fluorescence in Secs. V and VI, respectively. Section VII summarizes the study.

II. SYSTEM

Figure 1 shows the physical setup considered in this study. A quantum dot in a one-sided cavity is pumped by a continuous laser beam incident from the side. The overall system consists of the following elements: (i) a quantum dot, (ii) a cavity, (iii) a radiation field leaking from the cavity, (iv) noncavity radiation modes, and (v) the environment that causes pure dephasing of the dot. In this study, we treat these five elements as active quantum-mechanical degrees of freedom. Putting $\hbar = c = 1$, the Hamiltonian is given by

$$\mathcal{H} = \mathcal{H}_1 + \mathcal{H}_2 + \mathcal{H}_3 + \mathcal{H}_4, \tag{2}$$

$$\mathcal{H}_1 = \omega_d \sigma_{11} + \omega_c a^\dagger a + g(\sigma_{10} a + a^\dagger \sigma_{01}), \tag{3}$$

$$\mathcal{H}_2 = \int dk[k b_k^\dagger b_k + \sqrt{\kappa/(2\pi)}(a^\dagger b_k + b_k^\dagger a)], \tag{4}$$

$$\mathcal{H}_3 = \int dk[k c_k^\dagger c_k + \sqrt{\gamma/(2\pi)}(\sigma_{10} c_k + c_k^\dagger \sigma_{01})], \tag{5}$$

$$\mathcal{H}_4 = \int dk[k d_k^\dagger d_k + \sqrt{\gamma_p/\pi}\sigma_{11}(d_k^\dagger + d_k)], \tag{6}$$

where $\mathcal{H}_1$ describes the coherent interaction between the dot and the cavity (Jaynes-Cummings Hamiltonian [30]), $\mathcal{H}_2$ describes the leakage of cavity photons into the radiation pattern, $\mathcal{H}_3$ describes the radiative decay of the dot into noncavity modes, and $\mathcal{H}_4$ describes pure dephasing of the dot.

The parameters are defined as follows: ω_d and ω_c respectively denote the resonance frequencies of the dot and the cavity, g is the coherent coupling between them, κ is the cavity photon decay rate, γ is the radiative decay rate of the dot into noncavity modes, and γ_p is the pure-dephasing rate. The operators are defined as follows: The dot has ground and excited states ($|0\rangle$ and $|1\rangle$, respectively), and its transition operator is denoted by $\sigma_{ij} = |i\rangle\langle j|$. a is the annihilation operator of the cavity. b_k, c_k, and d_k respectively denote the field operators (wave-number representation) of leakage from the cavity, noncavity radiation modes, and the environment causing pure dephasing of the dot. The real-space representations of these operators are defined in terms of their Fourier transforms. For example,

$$\widetilde{b}_r = (2\pi)^{-1/2} \int dk e^{ikr} b_k. \tag{7}$$

In the real-space representations, the fields interact with the dot-cavity system at $r = 0$.

As illustrated in Fig. 1, we consider resonance fluorescence from the system pumped by a laser beam incident from the noncavity modes. At the initial time ($t = 0$), we assume that the pump has not arrived at the dot and that there are no other excitations in the overall system besides the pump light. Denoting the total vacuum state by $|0\rangle$, the initial state vector is given by

$$|\psi_i\rangle = \mathcal{N} \exp\left(\int dr E_{\rm in}(r)\widetilde{c}_r^\dagger\right)|0\rangle, \tag{8}$$

where $\mathcal{N} = \exp(-\int dr |E_{\rm in}(r)|^2/2)$ is a normalization constant and $E_{\rm in}(r)$ represents the pump light at the initial time, which is given by

$$E_{\rm in}(r) = \begin{cases} E e^{i\omega_p r} & (r < 0) \\ 0 & (0 < r), \end{cases} \tag{9}$$

where E is the pump amplitude and ω_p is the pump frequency. Note that $|\psi_i\rangle$ is in a coherent state and thus is an eigenstate of the initial field operators, satisfying $\widetilde{c}_r(0)|\psi_i\rangle = E_{\rm in}(r)|\psi_i\rangle$ and $\widetilde{b}_r(0)|\psi_i\rangle = \widetilde{d}_r(0)|\psi_i\rangle = 0$. It is often useful to characterize the pump amplitude by the Rabi frequency Ω, which is defined by

$$\Omega = 2\sqrt{\gamma}E. \tag{10}$$

Although we have modeled the noncavity radiation modes by a single continuum (c_k) for simplicity, they should in principle be modeled by many independent continua in order to reflect their in-plane directions. Furthermore, although we have modeled pure dephasing of the dot by coupling only $|1\rangle$ to the environment, in reality $|0\rangle$ also interacts with the environment and is subject to energy fluctuations. These extensions are straightforward and require redefining the parameters, but the essence of the theory remains the same.

III. HEISENBERG EQUATIONS

Throughout this study, our analysis is based on the Heisenberg equations that are derivable from the Hamiltonian of Eq. (2), together with the initial state vector of Eq. (8). The input-output relations connecting the incoming ($r < 0$) and outgoing ($r > 0$) fields are given by [31]

$$\widetilde{b}_r(t) = \widetilde{b}_{r-t}(0) - i\sqrt{\kappa}\theta(r)\theta(t-r)a(t-r), \tag{11}$$

$$\widetilde{c}_r(t) = \widetilde{c}_{r-t}(0) - i\sqrt{\gamma}\theta(r)\theta(t-r)\sigma_{01}(t-r), \tag{12}$$

$$\widetilde{d}_r(t) = \widetilde{d}_{r-t}(0) - i\sqrt{2\gamma_p}\theta(r)\theta(t-r)\sigma_{11}(t-r), \tag{13}$$

where $\theta(r)$ is the Heaviside step function. The Heisenberg equations for a, σ_{01}, and σ_{11} are given by

$$\frac{d}{dt}a = -i\widetilde{\omega}_c a - ig\sigma_{01} - iN_b(t), \tag{14}$$

$$\frac{d}{dt}\sigma_{01} = -i\widetilde{\omega}_d\sigma_{01} - ig(1-2\sigma_{11})a - i(1-2\sigma_{11})N_c(t) - i[N_d^\dagger(t)\sigma_{01} + \sigma_{01}N_d(t)], \quad (15)$$

$$\frac{d}{dt}\sigma_{11} = -\gamma\sigma_{11} + ig(a^\dagger\sigma_{01} - \sigma_{10}a) + i\left[N_c^\dagger(t)\sigma_{01} - \sigma_{10}N_c(t)\right], \quad (16)$$

where the complex frequencies of dot and cavity are defined respectively by $\widetilde{\omega}_d = \omega_d - i(\gamma/2+\gamma_p)$ and $\widetilde{\omega}_c = \omega_c - i\kappa/2$ and the noise operators are defined by $N_b(t) = \sqrt{\kappa}\widetilde{b}_{-t}(0)$, $N_c(t) = \sqrt{\gamma}\widetilde{c}_{-t}(0)$, and $N_d(t) = \sqrt{2\gamma_p}\widetilde{d}_{-t}(0)$. The Heisenberg equations for general system operators ($A_{0,0}^{m,n} = a^{\dagger m}a^n$, $A_{0,1}^{m,n} = \sigma_{01}a^{\dagger m}a^n$, and $A_{1,1}^{m,n} = \sigma_{11}a^{\dagger m}a^n$) are given by

$$\frac{d}{dt}A_{0,0}^{m,n} = \varepsilon_{0,0}^{m,n}A_{0,0}^{m,n} + ig\left(mA_{1,0}^{m-1,n} - nA_{0,1}^{m,n-1}\right) + i\left[mN_b^\dagger(t)A_{0,0}^{m-1,n} - nA_{0,0}^{m,n-1}N_b(t)\right], \quad (17)$$

$$\frac{d}{dt}A_{0,1}^{m,n} = \varepsilon_{0,1}^{m,n}A_{0,1}^{m,n} + ig\left(2A_{1,1}^{m,n+1} - A_{0,0}^{m,n+1} + mA_{1,1}^{m-1,n}\right) + i\left[mN_b^\dagger(t)A_{0,1}^{m-1,n} - nA_{0,1}^{m,n-1}N_b(t)\right] + i\left(2A_{1,1}^{m,n} - A_{0,0}^{m,n}\right)N_c(t) - i\left[N_d^\dagger(t)A_{0,1}^{m,n} + A_{0,1}^{m,n}N_d(t)\right], \quad (18)$$

$$\frac{d}{dt}A_{1,1}^{m,n} = \varepsilon_{1,1}^{m,n}A_{1,1}^{m,n} + ig\left(A_{0,1}^{m+1,n} - A_{1,0}^{m,n+1}\right) + i\left[mN_b^\dagger(t)A_{1,1}^{m-1,n} - nA_{1,1}^{m,n-1}N_b(t)\right] + i\left[N_c^\dagger(t)A_{0,1}^{m,n} - A_{1,0}^{m,n}N_c(t)\right], \quad (19)$$

where $\varepsilon_{\mu,v}^{m,n} = i(m-n)\omega_c - i(\mu-v)\omega_d - \frac{m+n}{2}\kappa - \frac{\mu+v}{2}\gamma - \delta_{\mu+v,1}\gamma_p$. The equation of motion for $A_{1,0}^{m,n}$ is given by $A_{1,0}^{m,n} = (A_{0,1}^{n,m})^\dagger$.

IV. CORRELATION FUNCTIONS

A. One-time correlation functions

In this section, we discuss the one- and two-time correlation functions of the system operators. The one-time correlation function can be evaluated immediately from the Heisenberg equations and the initial state vector. We discuss $\langle a(t)\rangle$ and $\langle\sigma_{01}(t)\rangle$ as examples. Generalization to other quantities, including higher-order ones, is straightforward. Since the noise operators can be replaced by c numbers as $N_b(t)|\psi_i\rangle = N_d(t)|\psi_i\rangle = 0$ and $N_c(t)|\psi_i\rangle = (\Omega/2)e^{-i\omega_p t}|\psi_i\rangle$, we have

$$\frac{d}{dt}\langle a\rangle = -i\widetilde{\omega}_c\langle a\rangle - ig\langle\sigma_{01}\rangle, \quad (20)$$

$$\frac{d}{dt}\langle\sigma_{01}\rangle = -i\widetilde{\omega}_d\langle\sigma_{01}\rangle - ig(\langle a\rangle - 2\langle\sigma_{11}a\rangle) - i\Omega e^{-i\omega_p t}(1/2 - \langle\sigma_{11}\rangle). \quad (21)$$

When stationary, $\langle\sigma_{\mu v}a^{\dagger m}a^n(t)\rangle$ evolves in time as $\langle\sigma_{\mu v}a^{\dagger m}a^n(t)\rangle = \langle\sigma_{\mu v}a^{\dagger m}a^n\rangle_s e^{i(m-n+\mu-v)\omega_p t}$, where $\langle\sigma_{\mu v}a^{\dagger m}a^n\rangle_s$ is a constant. We then have

$$0 = -i\widetilde{\omega}_c'\langle a\rangle_s - ig\langle\sigma_{01}\rangle_s, \quad (22)$$

$$i\Omega/2 = -i\widetilde{\omega}_d'\langle\sigma_{01}\rangle_s - ig(\langle a\rangle_s - 2\langle\sigma_{11}a\rangle_s) + i\Omega\langle\sigma_{11}\rangle_s, \quad (23)$$

where $\widetilde{\omega}_c' = \widetilde{\omega}_c - \omega_p$ and $\widetilde{\omega}_d' = \widetilde{\omega}_d - \omega_p$ are complex frequencies in the rotating frame. The above equations, together with those for other higher-order quantities, form a set of simultaneous inhomogeneous linear equations. Although these simultaneous equations involve an infinite number of variables, accurate numerical results can be obtained by considering up to 15 cavity photons.

B. Two-time correlation functions

As an example of a two-time correlation function, we investigate $\langle a^\dagger(t)a(t+\tau)\rangle$. This quantity becomes independent of t when stationary and the correlation between the two operators is lost in the $\tau\to\infty$ limit. Therefore, we can divide it into transient and stationary components as

$$\langle a^\dagger(t)a(t+\tau)\rangle = [\langle a^\dagger,a(\tau)\rangle + \langle a\rangle_s^*\langle a\rangle_s]e^{-i\omega_p\tau}. \quad (24)$$

The equation of motion for the transient component is derivable from Eq. (14). Since $\langle a^\dagger,a(-\tau)\rangle = \langle a^\dagger,a(\tau)\rangle^*$, we assume $\tau \geqslant 0$ in the following. Since the noise operators at $t+\tau$ commute with the system operators at t, we have

$$\frac{d}{d\tau}\langle a^\dagger,a(\tau)\rangle = -i\widetilde{\omega}_c'\langle a^\dagger,a(\tau)\rangle - ig\langle a^\dagger,\sigma_{01}(\tau)\rangle. \quad (25)$$

Thus, the equations of motion for the two-time functions are similar to those for the one-time functions. The initial and asymptotic values are given respectively by $\langle A,B(0)\rangle = \langle AB\rangle_s - \langle A\rangle_s\langle B\rangle_s$ and $\langle A,B(\infty)\rangle = 0$ for any two system operators.

As we see in Sec. V B, we are interested in the following integral:

$$I_{a^\dagger,a}(\omega) = \int_0^\infty d\tau\,\langle a^\dagger,a(\tau)\rangle e^{i(\omega-\omega_p)\tau}. \quad (26)$$

In order to evaluate this quantity compactly, we calculate $J_{a^\dagger,a}(\omega) = \int_0^\infty d\tau\,\frac{d}{d\tau}\langle a^\dagger,a(\tau)\rangle e^{i(\omega-\omega_p)\tau}$ in two ways. By partially integrating the right-hand side, we have $J_{a^\dagger,a}(\omega) = -\langle a^\dagger,a(0)\rangle - i(\omega-\omega_p)I_{a^\dagger,a}(\omega)$. On the other hand, by using Eq. (25), we have $J_{a^\dagger,a}(\omega) = -i\widetilde{\omega}_c'I_{a^\dagger,a}(\omega) - igI_{a^\dagger,\sigma_{01}}(\omega)$. From the above two equations, we obtain the following equation:

$$-\langle a^\dagger,a(0)\rangle = -i\widetilde{\omega}_c''I_{a^\dagger,a}(\omega) - igI_{a^\dagger,\sigma_{01}}(\omega), \quad (27)$$

where $\widetilde{\omega}_c'' = \widetilde{\omega}_c' - (\omega-\omega_p)$. This equation, together with those for other variables such as $I_{\sigma_{10},\sigma_{01}}(\omega)$, also forms a set of simultaneous inhomogeneous linear equations.

V. ANALYTIC RESULTS

In this section, we discuss how the system variables discussed in Sec. IV affect the output radiation properties such as its amplitude and power spectrum. We also express the photon and energy fluxes in terms of the system variables and observe how the photon number and energy are conserved between the input and output.

A. Coherent amplitude

We first discuss the coherent amplitudes of the output fields, which are defined as the one-time correlation functions of field operators by $E^b_{\rm out}(r,t) = \langle \widetilde{b}_r(t)\rangle$, $E^c_{\rm out}(r,t) = \langle \widetilde{c}_r(t)\rangle$, and $E^d_{\rm out}(r,t) = \langle \widetilde{d}_r(t)\rangle$. Such amplitudes can, in principle, be measured by homodyne measurements and yield the coherent components in the power spectra. From Eqs. (11)–(13) and (8), we have in the stationary state ($t \to \infty$)

$$E^b_{\rm out}(r,t) = -i\sqrt{\kappa}\langle a\rangle_s e^{i\omega_p(r-t)}, \tag{28}$$

$$E^c_{\rm out}(r,t) = (E - i\sqrt{\gamma}\langle\sigma_{01}\rangle_s)e^{i\omega_p(r-t)}, \tag{29}$$

$$E^d_{\rm out}(r,t) = -i\sqrt{2\gamma_p}\langle\sigma_{11}\rangle_s. \tag{30}$$

Note that the input wave is superimposed on the emission from the system in $E^c_{\rm out}$, whereas $E^b_{\rm out}$ and $E^d_{\rm out}$ consist only of the emission.

B. Power spectrum

The power spectrum $S^b(\omega)$ of cavity emission is defined as the Fourier transform of the two-time correlation function in the b field. It is given by

$$S^b(\omega) = \lim_{T\to\infty}\iint_0^T \frac{dt_1 dt_2}{2\pi T} e^{i\omega(t_2-t_1)}\langle \widetilde{b}^\dagger_r(t_1)\widetilde{b}_r(t_2)\rangle, \tag{31}$$

where r (>0) represents the detector position. Since the two-time correlation function depends only on the difference in time when stationary, the above equation is rewritten as

$$S^b(\omega) = {\rm Re}\int_0^\infty \frac{d\tau}{\pi} e^{i\omega\tau}\langle \widetilde{b}^\dagger_r(t)\widetilde{b}_r(t+\tau)\rangle, \tag{32}$$

where $t \gg r$. Using the results of Sec. IV B, we can divide the spectrum into coherent and incoherent components as $S^b(\omega) = S^b_{\rm coh}(\omega) + S^b_{\rm inc}(\omega)$, where

$$S^b_{\rm coh}(\omega) = \left|E^b_{\rm out}\right|^2\delta(\omega-\omega_p), \tag{33}$$

$$S^b_{\rm inc}(\omega) = (\kappa/\pi){\rm Re}[I_{a^\dagger,a}(\omega)]. \tag{34}$$

Repeating the same arguments, $S^c(\omega)$ and $S^d(\omega)$ are also divided into coherent and incoherent components. They are given by

$$S^c_{\rm coh}(\omega) = \left|E^c_{\rm out}\right|^2\delta(\omega-\omega_p), \tag{35}$$

$$S^c_{\rm inc}(\omega) = (\gamma/\pi){\rm Re}[I_{\sigma_{10},\sigma_{01}}(\omega)], \tag{36}$$

$$S^d_{\rm coh}(\omega) = \left|E^d_{\rm out}\right|^2\delta(\omega), \tag{37}$$

$$S^d_{\rm inc}(\omega) = (2\gamma_p/\pi){\rm Re}[I_{\sigma_{11},\sigma_{11}}(\omega)]. \tag{38}$$

C. Flux conservation

The photon flux corresponding to $S^b_{\rm inc}(\omega)$ is defined by $\mathcal{F}^b_{\rm inc} = \int d\omega S^b_{\rm inc}(\omega)$. This quantity can be evaluated as follows. From Eqs. (26) and (34), $S^b_{\rm inc}(\omega)$ is rewritten as

$$S^b_{\rm inc}(\omega) = \frac{\kappa}{\pi}{\rm Re}\int_0^\infty d\tau e^{i(\omega-\omega_p)\tau}\langle a^\dagger, a(\tau)\rangle. \tag{39}$$

By integrating this equation with respect to ω, $\mathcal{F}^b_{\rm inc}$ is obtained as $\mathcal{F}^b_{\rm inc} = \kappa\langle a^\dagger, a(0)\rangle = \kappa\langle a^\dagger a\rangle_s - \kappa|\langle a\rangle_s|^2$. Repeating similar calculations, other flux components can be expressed in terms of the stationary system variables as

$$\mathcal{F}^b_{\rm coh} = \kappa|\langle a\rangle_s|^2, \tag{40}$$

$$\mathcal{F}^b_{\rm inc} = \kappa\langle a^\dagger a\rangle_s - \kappa|\langle a\rangle_s|^2, \tag{41}$$

$$\mathcal{F}^c_{\rm coh} = |E - i\sqrt{\gamma}\langle\sigma_{01}\rangle_s|^2, \tag{42}$$

$$\mathcal{F}^c_{\rm inc} = \gamma\langle\sigma_{11}\rangle_s - \gamma|\langle\sigma_{01}\rangle_s|^2, \tag{43}$$

$$\mathcal{F}^d_{\rm coh} = 2\gamma_p\langle\sigma_{11}\rangle_s^2, \tag{44}$$

$$\mathcal{F}^d_{\rm inc} = 2\gamma_p(\langle\sigma_{11}\rangle_s - \langle\sigma_{11}\rangle_s^2). \tag{45}$$

We can confirm that

$$\mathcal{F}^b_{\rm coh} + \mathcal{F}^b_{\rm inc} + \mathcal{F}^c_{\rm coh} + \mathcal{F}^c_{\rm inc} = E^2. \tag{46}$$

This represents the flux (number) conservation law since E^2 is the input flux. Therefore, for example, $\mathcal{F}^b_{\rm inc}/E^2$ represents the probability of the pump light being inelastically scattered into the b field.

D. Energy conservation

The energy flux corresponding to $S^b_{\rm inc}(\omega)$ is defined by $\mathcal{E}^b_{\rm inc} = \int d\omega\ \omega S^b_{\rm inc}(\omega)$. This quantity can be evaluated as follows: Using Eq. (39), $\omega S^b_{\rm inc}(\omega)$ can be rewritten as

$$\omega S^b_{\rm inc}(\omega) = \frac{\kappa\omega_p}{\pi}{\rm Re}\int_0^\infty d\tau e^{i(\omega-\omega_p)\tau}\langle a^\dagger, a(\tau)\rangle + \frac{\kappa}{\pi}{\rm Im}\int_0^\infty d\tau e^{i(\omega-\omega_p)\tau}\frac{d}{d\tau}\langle a^\dagger, a(\tau)\rangle. \tag{47}$$

$\mathcal{E}^b_{\rm inc}$ is obtained by integrating this equation with respect to ω. The first term yields $\omega_p\mathcal{F}^b_{\rm inc}$. The second term can be rewritten as $\kappa{\rm Re}[\omega_c'\langle a^\dagger, a(0)\rangle + g\langle a^\dagger, \sigma_{01}(0)\rangle]$ using Eq. (25), which is further simplified as $\kappa\omega_c'\langle a^\dagger a\rangle_s + \kappa g(\langle a^\dagger\sigma_{01}\rangle_s + {\rm c.c.})/2$ using Eq. (20). Thus, $\mathcal{E}^b_{\rm inc} = \kappa\omega_c\langle a^\dagger a\rangle_s + \frac{\kappa g}{2}(\langle a^\dagger\sigma_{01}\rangle_s + {\rm c.c.}) - \kappa\omega_p|\langle a\rangle_s|^2$. Repeating similar calculations, other energy flux components can be expressed in terms of the stationary system variables as

$$\mathcal{E}^b_{\rm coh} = \omega_p\mathcal{F}^b_{\rm coh}, \tag{48}$$

$$\mathcal{E}^b_{\rm inc} = \kappa\omega_c\langle a^\dagger a\rangle_s + \frac{\kappa g}{2}(\langle a^\dagger\sigma_{01}\rangle_s + {\rm c.c.}) - \mathcal{E}^b_{\rm coh}, \tag{49}$$

$$\mathcal{E}^c_{\rm coh} = \omega_p\mathcal{F}^c_{\rm coh}, \tag{50}$$

$$\mathcal{E}^c_{\rm inc} = \omega_p|E|^2 + \gamma\omega_d\langle\sigma_{11}\rangle_s + \left[\frac{\gamma g}{2}\langle\sigma_{10}a\rangle_s + \sqrt{\gamma}E(\gamma/2 + i\omega_p)\langle\sigma_{10}\rangle_s + {\rm c.c.}\right] - \mathcal{E}^c_{\rm coh}, \tag{51}$$

$$\mathcal{E}^d_{\rm coh} = 0, \tag{52}$$

$$\mathcal{E}^d_{\rm inc} = \gamma_p(g\langle\sigma_{10}a\rangle_s + \sqrt{\gamma}E\langle\sigma_{10}\rangle_s + {\rm c.c.}). \tag{53}$$

We can confirm that

$$\mathcal{E}^b_{\rm coh} + \mathcal{E}^b_{\rm inc} + \mathcal{E}^c_{\rm coh} + \mathcal{E}^c_{\rm inc} + \mathcal{E}^d_{\rm inc} = \omega_p E^2. \tag{54}$$

This represents the energy conservation law since $\omega_p E^2$ represents the energy flux of the input pump. It differs remarkably from the flux conservation law of Eq. (46) in that the input energy is not necessarily conserved within the light fields (b and c fields). Equation (53) indicates that $\mathcal{E}^d_{\rm inc}$ may become nonzero when pure dephasing occurs ($\gamma_p \neq 0$).

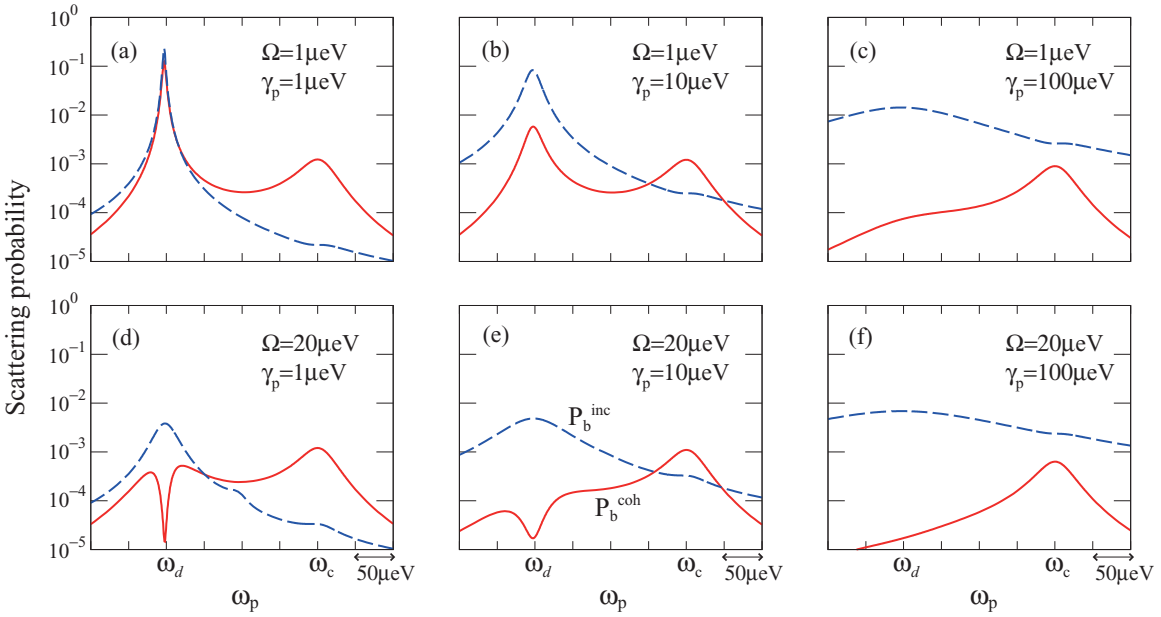

FIG. 2. (Color online) Probabilities of elastic scattering (solid lines) and inelastic scattering (dashed lines) to the b field as functions of the pump frequency. Pump intensity and pure dephasing rate are indicated in each panel. Other parameters are as follows: $\omega_c - \omega_d = 200\ \mu$eV, $g = 25\ \mu$eV, $\kappa = 50\ \mu$eV, and $\gamma = 1\ \mu$eV.

This implies that the pump light can continuously absorb energy from the environment ($\mathcal{E}^d_{\rm inc} < 0$) or release energy to the environment ($\mathcal{E}^d_{\rm inc} > 0$) as a result of inelastic scattering.

VI. NUMERICAL RESULTS

A. Scattering probabilities to *b* field

We present the numerical results in this section. To discuss the nonresonant coupling between the dot and the cavity, we assume that the system has a large dot-cavity detuning and is in the weak-coupling regime. We first consider the probabilities of elastic and inelastic scattering to the b field. From the flux sum rule of Eq. (46), they are defined by $\mathcal{P}^b_{\rm coh} = \mathcal{F}^b_{\rm coh}/E^2$ and $\mathcal{P}^b_{\rm inc} = \mathcal{F}^b_{\rm inc}/E^2$. In the present configuration, most of the input pump light is output coherently in the c field and only a small fraction is scattered to the b field. Figures 2(a)–2(c) show the results for a weak pump for three different values of the pure dephasing rate γ_p. $\mathcal{P}^b_{\rm inc}$ has a single peak at ω_d, whereas $\mathcal{P}^b_{\rm coh}$ has two peaks at ω_d and ω_c. The peak at ω_d has a width of $\gamma/2 + \gamma_p$ and is therefore broadened as γ_p is

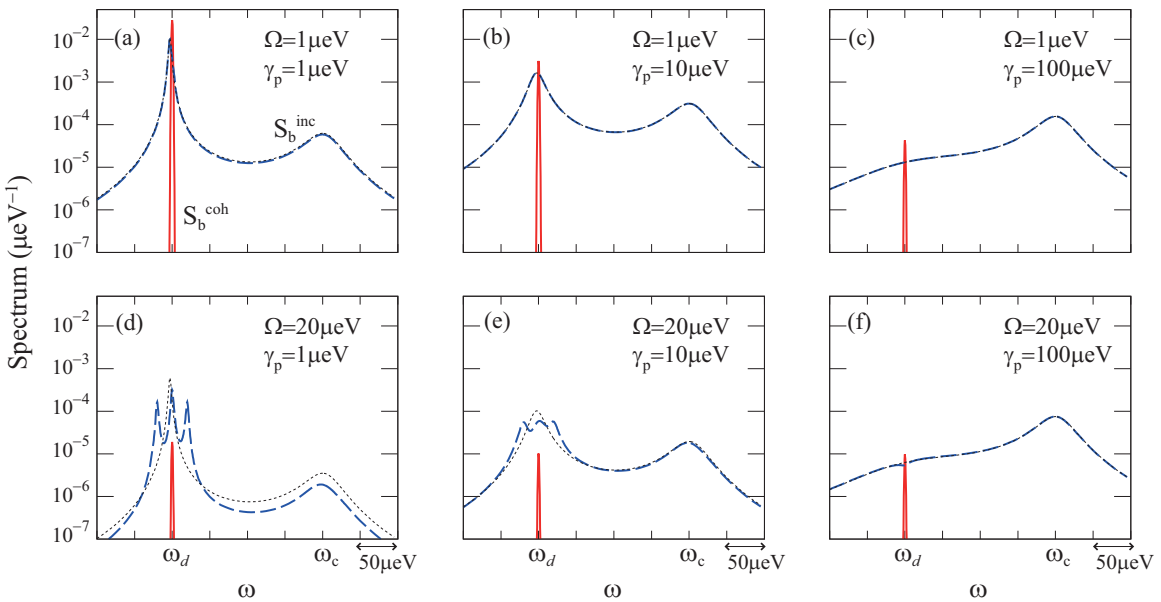

FIG. 3. (Color online) Power spectrum of radiation in the b field: coherent component (solid lines), incoherent component (dashed lines), and spontaneous emission (thin dotted lines). The pump is tuned to the dot ($\omega_p = \omega_d$). Other parameters are the same as those in Fig. 2. $S^b_{\rm inc}$ and $S^b_{\rm se}$ overlap in (a)–(c) and (f).

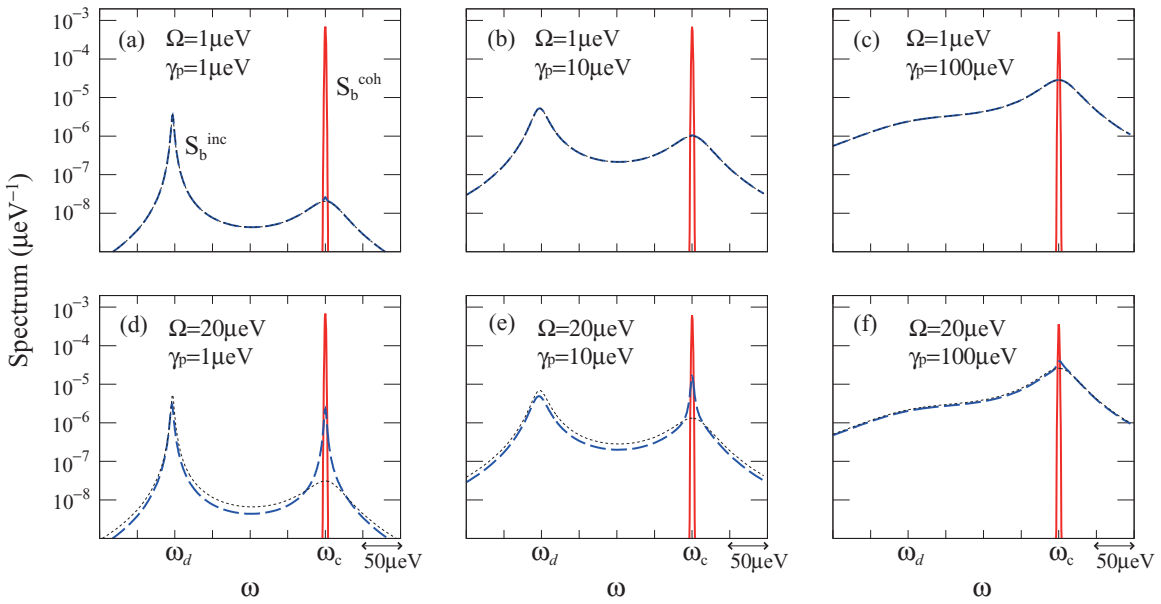

FIG. 4. (Color online) Same plots as Fig. 3 but for pumping at the cavity frequency ($\omega_p = \omega_c$). $S^b_{\rm inc}$ and $S^b_{\rm se}$ overlap in (a)–(c) and (f).

increased, whereas the peak at ω_c has a width of $\kappa/2$ and is therefore unaffected. As expected, inelastic scattering ($\mathcal{P}^b_{\rm inc}$) becomes increasingly dominant as γ_p increases.

Figures 2(d)–2(f) show the results for a strong pump. The scattering probabilities remain almost the same as those for a weak pump when the pump is out of resonance with the dot. However, in contrast with the weak-pump cases, $\mathcal{P}^b_{\rm coh}$ is drastically suppressed near the dot frequency, as observed in Figs. 2(d) and 2(e). As we will see later, the energy level of the dot is Rabi split under a strong pump. The sharp dip can be attributed to destructive interference of waves scattered elastically by these two levels.

B. Power spectrum in *b* field

We now discuss the power spectrum of light scattered to the b field. The spectrum is composed of coherent and incoherent components, as given by Eqs. (33) and (34), respectively. They are plotted after normalization [$\int d\omega S^b_{\rm coh}(\omega) = \mathcal{P}^b_{\rm coh}$ and $\int d\omega S^b_{\rm inc}(\omega) = \mathcal{P}^b_{\rm inc}$] in Figs. 3 and 4. To visualize the coherent component, which is a delta function in principle, we replaced it with a Gaussian function, $S^b_{\rm coh}(\omega) = \mathcal{P}^b_{\rm coh}\exp[-(\omega-\omega_p)^2/\Delta^2]/(\sqrt{\pi}\Delta)$, where Δ (=1 μeV) is an artificially introduced width. We cannot obtain a compact analytic expression for the incoherent component $S^b_{\rm inc}$ since it is determined after solving a set of simultaneous equations involving an infinite number of variables. However, we expect that $S^b_{\rm inc}$ will be similar to the spontaneous-emission spectrum $S_{\rm se}$ of Eq. (1). Therefore, we also plot $S^b_{\rm se}$ as a reference for $S^b_{\rm inc}$ after normalization [$\int d\omega S^b_{\rm se}(\omega) = \mathcal{P}^b_{\rm inc}$].

Figure 3 shows the results for pumping at the dot frequency ($\omega_p = \omega_d$). $S^b_{\rm inc}$ agrees well with $S_{\rm se}$, particularly for the weak-pump cases of Figs. 3(a)–3(c). Therefore, radiation in the b field consists of elastically scattered light and spontaneous emission from the excited dot, and their strengths are determined by Eqs. (40) and (41). This simple picture breaks down for stronger inputs. Rabi splitting of the dot ($\Omega = 20$ μeV) is clearly visible in Figs. 3(d) and 3(e). This splitting is smeared out as the dot linewidth is increased, as observed in Fig. 3(f). For pumping at the dot resonance, the incoherent component generally dominates the coherent component in the b field (see Fig. 2) and, consequently, the whole spectrum $S_b = S^b_{\rm coh} + S^b_{\rm inc}$ is governed by the incoherent component. When the pure dephasing rate is large, the peak at ω_c may become larger than the peak at the pump frequency ω_d even when the elastic component is included.

Figure 4 shows the results for pumping at the cavity frequency ($\omega_p = \omega_c$). It is observed again that $S^b_{\rm inc}$ agrees well with $S_{\rm se}$, particularly for the weak-pump cases of Figs. 4(a)–4(c). However, deviations are apparent between $S^b_{\rm inc}$ and $S_{\rm se}$ in the strong-pumping cases of Figs. 4(d)–4(f). The incoherent emission close to the pump frequency is drastically enhanced. This is due to stimulated emission of the dot induced by the strong elastically scattered light. When pumping at the cavity resonance, the coherent component generally dominates the incoherent component in the b field (see Fig. 2) and, therefore, the peak at the pump frequency is always larger than the peak at ω_d.

C. Energy exchange with the environment

As discussed in Sec. V D, the pump light can exchange energy with the environment: a negative $\mathcal{E}^d_{\rm inc}$ indicates absorption of energy from the environment, whereas a positive $\mathcal{E}^d_{\rm inc}$ indicates emission. This exchanged energy per unit pump flux ($\mathcal{E}^d_{\rm inc}/E^2$) is plotted as a function of ω_p in Fig. 5. This figure reveals that effective energy exchange occurs for pumping near the dot frequency. This is because energy exchange occurs as a result of inelastic scattering and the probability of inelastic scattering is large near the dot resonance, as observed in Fig. 2. For pumping at the dot frequency, the light frequency becomes closer to the cavity frequency after inelastic scattering, as Fig. 3 shows. Therefore, the pump

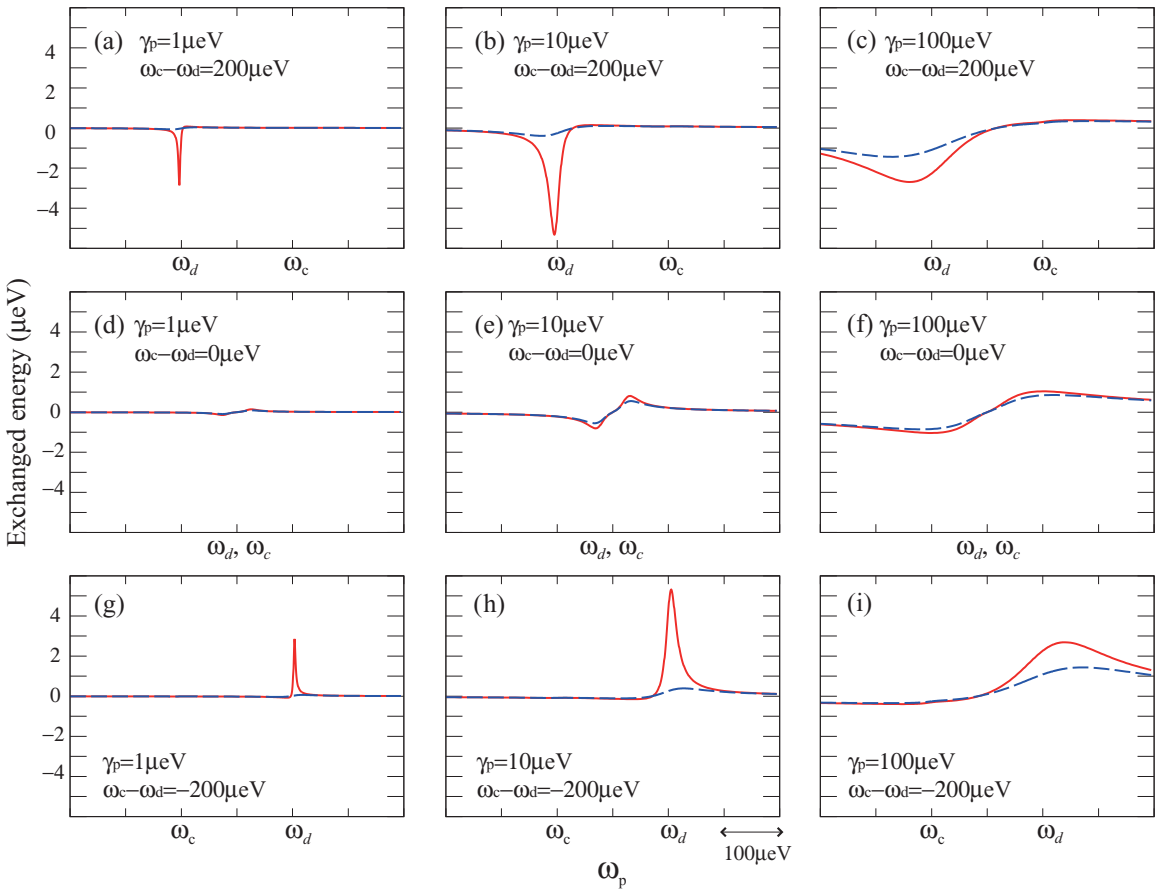

FIG. 5. (Color online) Plots of energy exchanged with the environment ($\mathcal{E}^d_{\rm inc}/E^2$) as functions of the pump frequency ω_p. The values of γ_p and $\omega_d - \omega_c$ are indicated in each panel. Solid lines indicate weak pumping ($\Omega = 1$ μeV) and dashed lines show strong pumping ($\Omega = 20$ μeV). Other parameters are as follows: $g = 25$ μeV, $\kappa = 50$ μeV, and $\gamma = 1$ μeV.

light absorbs energy when $\omega_d < \omega_c$, whereas it emits energy when $\omega_d > \omega_c$. When $\omega_c \sim \omega_d$, energy exchange becomes ineffective since the frequency shifts only slightly on inelastic scattering. These results indicate an interesting possibility of laser cooling of solid-state optical systems by utilizing pure-dephasing coupling with the environment. However, although not considered explicitly in this study, an excited dot may decay nonradiatively and release its energy to the environment. Consequently, whether laser cooling will occur will depend on the rates of pure dephasing and nonradiative decay.

We discuss here the relationship between the existing scheme for solid-state laser cooling using ytterbium- or thulium-doped glass [32,33] and the current scheme. In the scheme of Refs. [32,33], the mean energy of emission from the solid is determined by the electronic structure of this material. When the pump energy is lower (higher) than this mean energy, the pumping results in cooling (heating) of the solid. In contrast, in the current scheme, the mean energy of emission from the dot is sensitive to its dielectric environment, which can be controlled by the cavity resonance. A cavity enhances the coupling between the dot and the radiation field in the frequency region close to its resonance. Therefore, when $\omega_c > \omega_d$ ($\omega_c < \omega_d$), the dot tends to emit blue- (red-)shifted photons and the pumping results in cooling (heating) of the solid.

VII. SUMMARY

In this study, we theoretically investigated resonance fluorescence from a solid-state cavity QED system. We employed a model in which all the elements of the system (including environmental ones) are treated as active quantum-mechanical degrees of freedom. By rigorously solving the resultant Heisenberg equations, we revealed the properties of output light, such as the probabilities of elastic and inelastic scattering, the power spectrum, and the energy exchanged with the environment. In particular, we focused on cases with large dot-cavity detuning and observed the effects of pure dephasing. The results are summarized as follows: (i) The incoherent component of the power spectrum agrees well with the spontaneous-emission spectrum for a weak pump. Using a stronger pump results in Rabi splitting and stimulated emission near the pump frequency. (ii) Pure dephasing enhances the nonresonant coupling between the dot and the cavity and yields strong emission at the cavity frequency, as observed in experiments. (iii) The pump light exchanges energy with the environment that causes pure dephasing of the dot. Under appropriate conditions, the pump can continuously absorb energy from the environment, indicating the possibility of laser cooling in solid-state optical systems.

ACKNOWLEDGMENTS

The author is grateful to E. Iyoda, K. Kato, and Y. Nakamura for fruitful discussions. This research was partially supported by MEXT KAKENHI (Grants No. 23104710 and No. 22244035), Strategic Information and Communications R & D Promotion Program (SCOPE No. 111507004) of the Ministry of Internal Affairs and Communications, and National Institute of Information and Communications Technology (NICT).

[1] C. K. Hong, Z. Y. Ou, and L. Mandel, Phys. Rev. Lett. **59**, 2044 (1987).
[2] C. Santori *et al.*, Nature (London) **419**, 594 (2002).
[3] M. Keller *et al.*, Nature (London) **431**, 1075 (2004).
[4] J. McKeever *et al.*, Science **303**, 1992 (2004).
[5] B. Darquie *et al.*, Science **309**, 454 (2005).
[6] E. M. Purcell, Phys. Rev. **69**, 681 (1946).
[7] J. M. Raimond, M. Brune, and S. Haroche, Rev. Mod. Phys. **73**, 565 (2001).
[8] R. Miller *et al.*, J. Phys. B **38**, S551 (2005).
[9] T. Aoki, A. S. Parkins, D. J. Alton, C. A. Regal, B. Dayan, E. Ostby, K. J. Vahala, and H. J. Kimble, Phys. Rev. Lett. **102**, 083601 (2009).
[10] A. Muller, E. B. Flagg, P. Bianucci, X. Y. Wang, D. G. Deppe, W. Ma, J. Zhang, G. J. Salamo, M. Xiao, and C. K. Shih, Phys. Rev. Lett. **99**, 187402 (2007).
[11] D. Englund, D. Fattal, E. Waks, G. Solomon, B. Zhang, T. Nakaoka, Y. Arakawa, Y. Yamamoto, and J. Vuckovic, Phys. Rev. Lett. **95**, 013904 (2005).
[12] A. Blais, R. S. Huang, A. Wallraff, S. M. Girvin, and R. J. Schoelkopf, Phys. Rev. A **69**, 062320 (2004).
[13] M. H. Devoret, S. Girvin, and R. Schoelkopf, Ann. Phys. (NY) **16**, 767 (2007).
[14] O. Astafiev *et al.*, Science **327**, 840 (2010).
[15] T. Yoshie *et al.*, Nature (London) **432**, 200 (2004).
[16] S. Strauf, K. Hennessy, M. T. Rakher, Y. S. Choi, A. Badolato, L. C. Andreani, E. L. Hu, P. M. Petroff, and D. Bouwmeester, Phys. Rev. Lett. **96**, 127404 (2006).
[17] M. Kaniber, A. Laucht, A. Neumann, J. M. Villas-Boas, M. Bichler, M. C. Amann, and J. J. Finley, Phys. Rev. B **77**, 161303 (2008).
[18] S. Ates *et al.*, Nat. Photon. **3**, 724 (2009).
[19] D. Englund, A. Majumdar, A. Faraon, M. Toishi, N. Stoltz, P. Petroff, and J. Vuckovic, Phys. Rev. Lett. **104**, 073904 (2010).
[20] A. Naesby, T. Suhr, P. T. Kristensen, and J. Mørk, Phys. Rev. A **78**, 045802 (2008).
[21] M. Yamaguchi, T. Asano, and S. Noda, Opt. Express **16**, 18607 (2008).
[22] A. Auffèves, Jean-Michel Gérard, and J.-P. Poizat, Phys. Rev. A **79**, 053838 (2009).
[23] R. J. Glauber, in *Quantum Optics and Electronics*, edited by C. de Witt, A. Blandin, and C. Cohen-Tannoudji (Gordon and Breach, New York, 1965), pp. 65–185.
[24] M. J. Gagen and G. J. Milburn, Phys. Rev. A **45**, 5228 (1992).
[25] G. J. Milburn and M. J. Gagen, Phys. Rev. A **46**, 1578 (1992).
[26] M. Brune, S. Haroche, V. Lefevre, J. M. Raimond, and N. Zagury, Phys. Rev. Lett. **65**, 976 (1990).
[27] M. Brune, S. Haroche, J. M. Raimond, L. Davidovich, and N. Zagury, Phys. Rev. A **45**, 5193 (1992).
[28] L. Davidovich, M. Brune, J. M. Raimond, and S. Haroche, Phys. Rev. A **53**, 1295 (1996).
[29] R. Onofrio and L. Viola, Phys. Rev. A **58**, 69 (1998).
[30] E. T. Jaynes and F. W. Cummings, Proc. IEEE **51**, 89 (1963).
[31] D. F. Walls and G. J. Milburn, *Quantum Optics* (Springer, New York, 1995), Sec. 7.1.
[32] R. I. Epstein *et al.*, Nature (London) **377**, 500 (1995).
[33] C. W. Hoyt, M. Sheik-Bahae, R. I. Epstein, B. C. Edwards, and J. E. Anderson, Phys. Rev. Lett. **85**, 3600 (2000).